ARTICLE

ELECTRONIC SUPPLEMENTARY INFORMATION

Contribution of photocatalytic and Fenton-based processes in nanotwin structured anodic TiO_2 nanotube layers modified by Ce and V

Guru Karthikeyan Thirunavukkarasu,[a†] Sridhar Gowrisankaran,[a†] Maria Caplovicova,[b] Leonid Satrapinskyy,[c] Maros Gregor,[c] Aleksandra Lavrikova,[d] Jan Gregus,[c] Radoslav Halko,[e] Gustav Plesch,[a] Martin Motola [a] and Olivier Monfort [*a]

[a.] *Department of Inorganic Chemistry, Faculty of Natural Sciences, Comenius University in Bratislava, Ilkovicova 6, Mlynska Dolina, 84215 Bratislava, Slovakia.*
[b.] *STU Center for Nanodiagnostics, Faculty of Materials Science and Technology in Trnava, Slovak University of Technology in Bratislava, Vazovova 5, 81243 Bratislava, Slovakia.*
[c.] *Department of Experimental Physics, Faculty of Mathematics Physics and Informatics, Comenius University in Bratislava, Mlynska Dolina, 84248 Bratislava, Slovakia.*
[d.] *Division of Environmental Physics, Faculty of Mathematics Physics and Informatics, Comenius University in Bratislava, Mlynska Dolina, 84248 Bratislava, Slovakia.*
[e.] *Department of Analytical Chemistry, Faculty of Natural Sciences, Comenius University in Bratislava, Ilkovicova 6, Mlynska Dolina, 84215 Bratislava, Slovakia.*

[†]These authors have contributed equally to the work.
[*]Corresponding author: Dr. Olivier Monfort; monfort1@uniba.sk; +421(0)290142141

Table S1: Experimental conditions for ICP-MS analysis.

	Parameters	**Settings**
Gas flow (L min^{-1})	Plasma flow	15.0
	Auxiliary flow	1.65
	Nebulizer flow	1.00
	Sheath flow	0,14
CRI Gases (mL min^{-1})	Skimmer (with He)	0
	Skimmer (with H_2)	0
RF	RF Power (kW)	1.30
Sample Introduction	Sampling depth (mm)	6.5
	Pump rate (rpm)	5
	Stabilization time (s)	90
	Spray chamber (°C)	3
Ion Optics (volts)	1st Extraction lens	-1
	2nd Extraction lens	-85
	3rd Extraction lens	-175
	Corner lens	-197
	Mirror lens left	22
	Mirror lens right	25
	Mirror lens bottom	25
	Entrance lens	0
	Entrance plate	-10
	Fringe bias	-1.0
	Pole bias	0
Quadrupole scan	Scan mode	Peak hopping
	Dwell time (ms)	20
	Points per peak	1
	Scans/Replicate	50
	Replicates/Sample	5

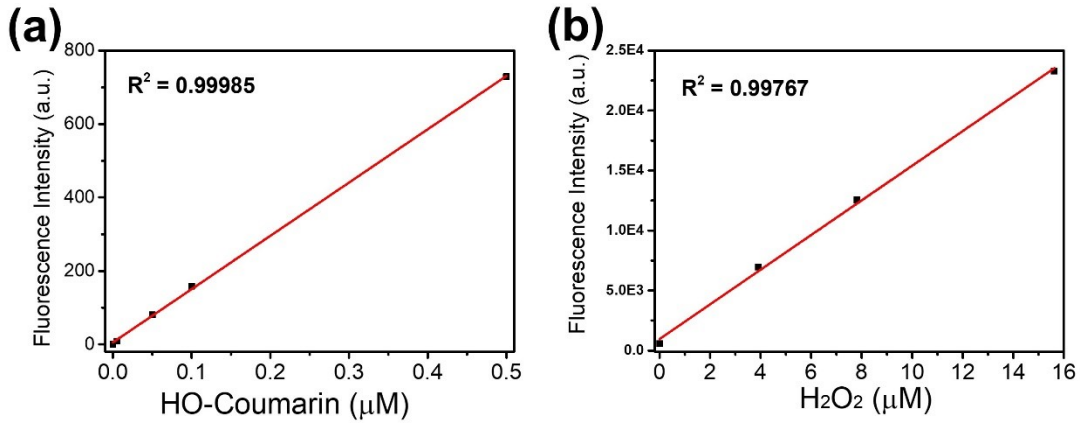

Figure S1: (a) Standard curve for $HO^{\bullet}$ detection i.e. using different concentrations of fluorescent hydroxycoumarin (since coumarin is the probe molecule). (b) Standard curve for H_2O_2 detection i.e. using different concentrations of H_2O_2 in the presence hydroxyphenylacetic acid as probe molecule (thus forming fluorescent HPAA dimer in the presence of peroxidase).

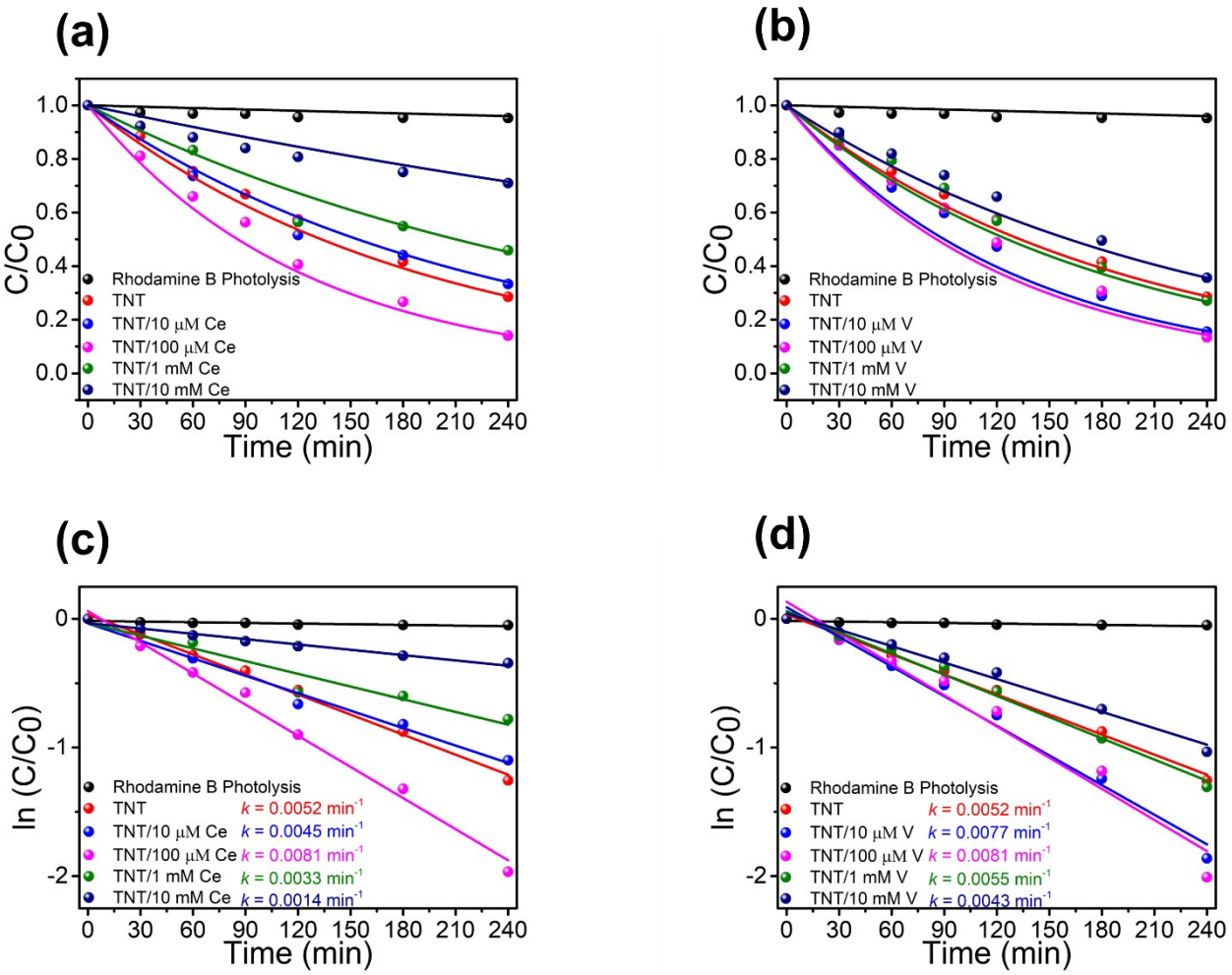

Figure S2: Optimization of Rhodamine B photodegradation at normal pH (i.e. pH was not altered) with a different surface dopant concentration of Ce or V on TNT. (a) & (b) C/C_0 of Ce doped TNT and V doped TNT, respectively. (c) & (d) Linearized pseudo-first-order plots of ln (C/C_0) versus time for Ce doped TNT and V doped TNT, respectively.

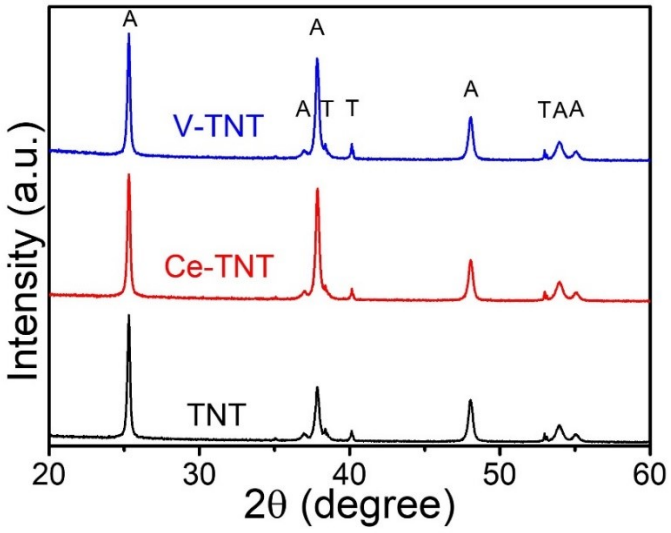

Figure S3: XRD patterns of TNT, Ce-TNT and V-TNT. The diffraction patterns labelled as A and T denotes TiO_2 anatase phase and metallic Ti, respectively.

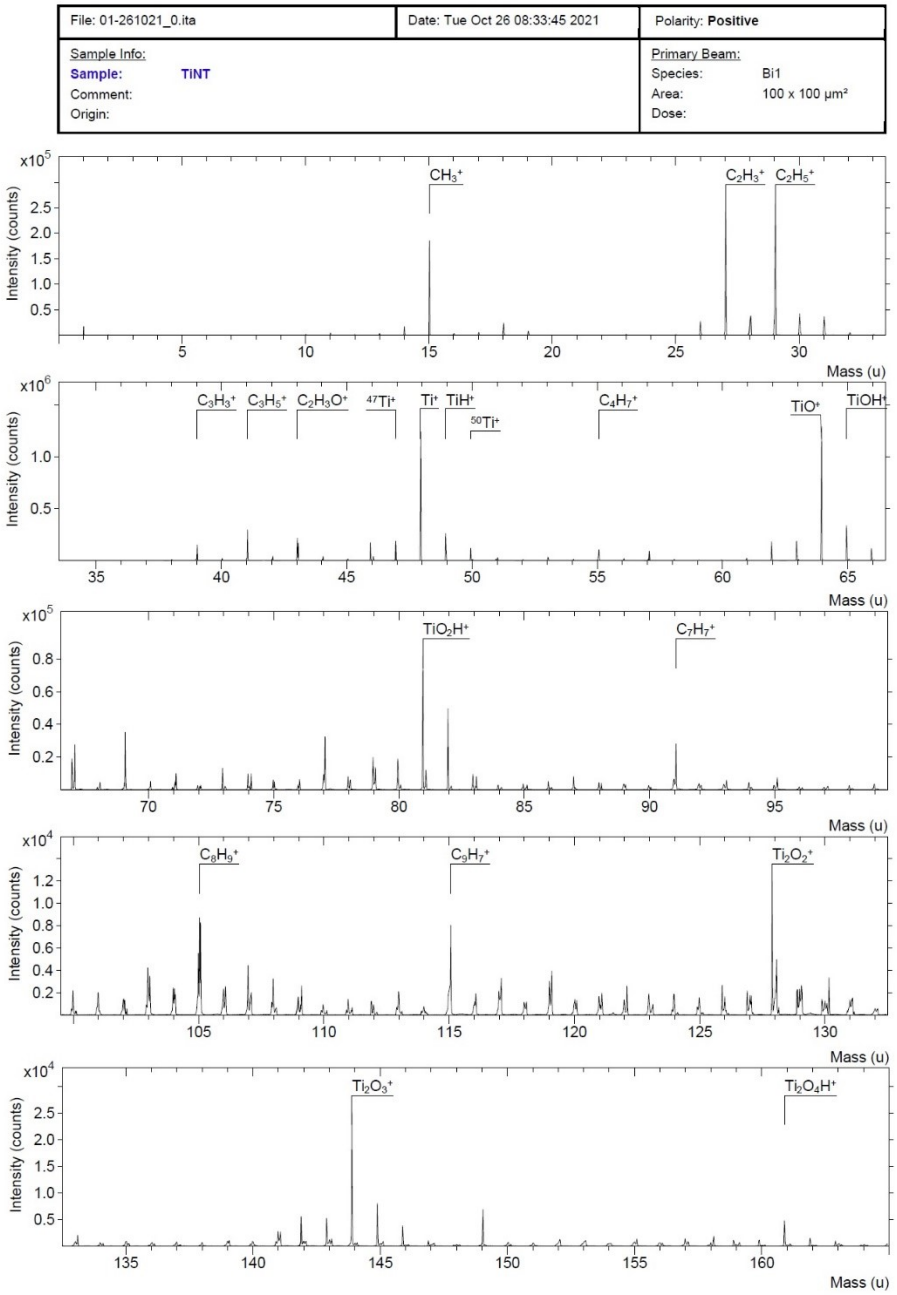

Figure S4a: SIMS of TNT.

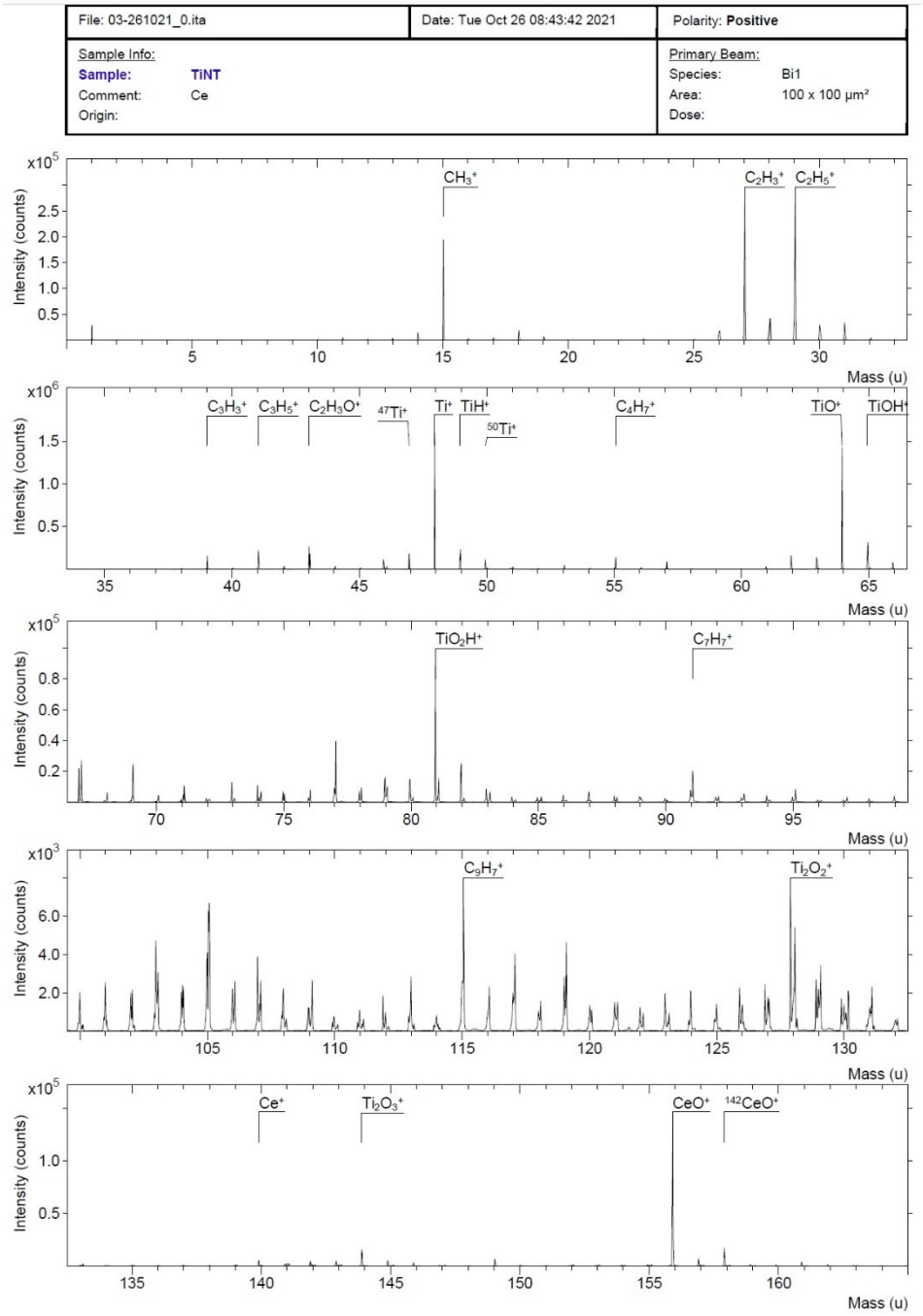

Figure S4b: SIMS of Ce-TNT.

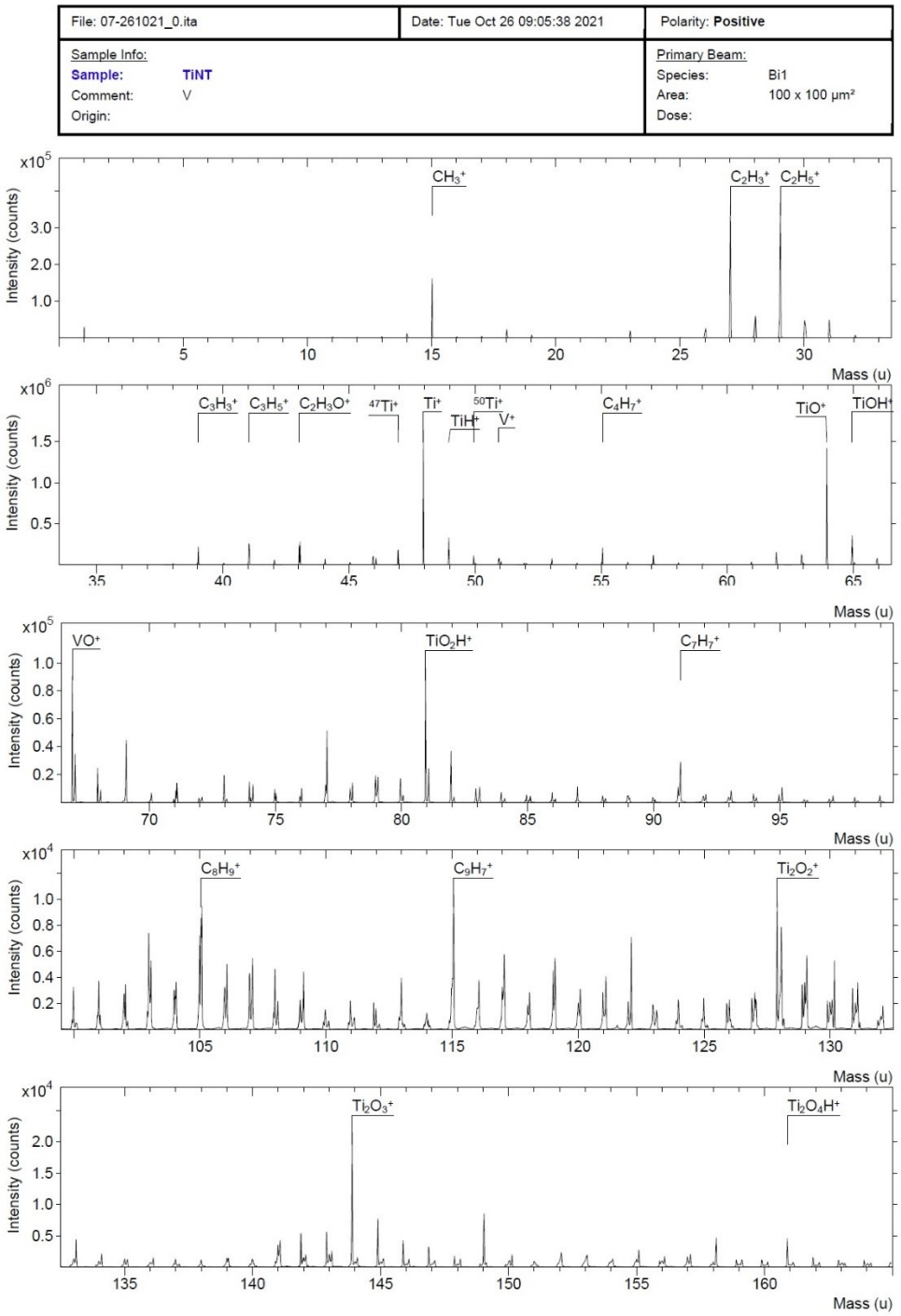

Figure S4c: SIMS of V-TNT.

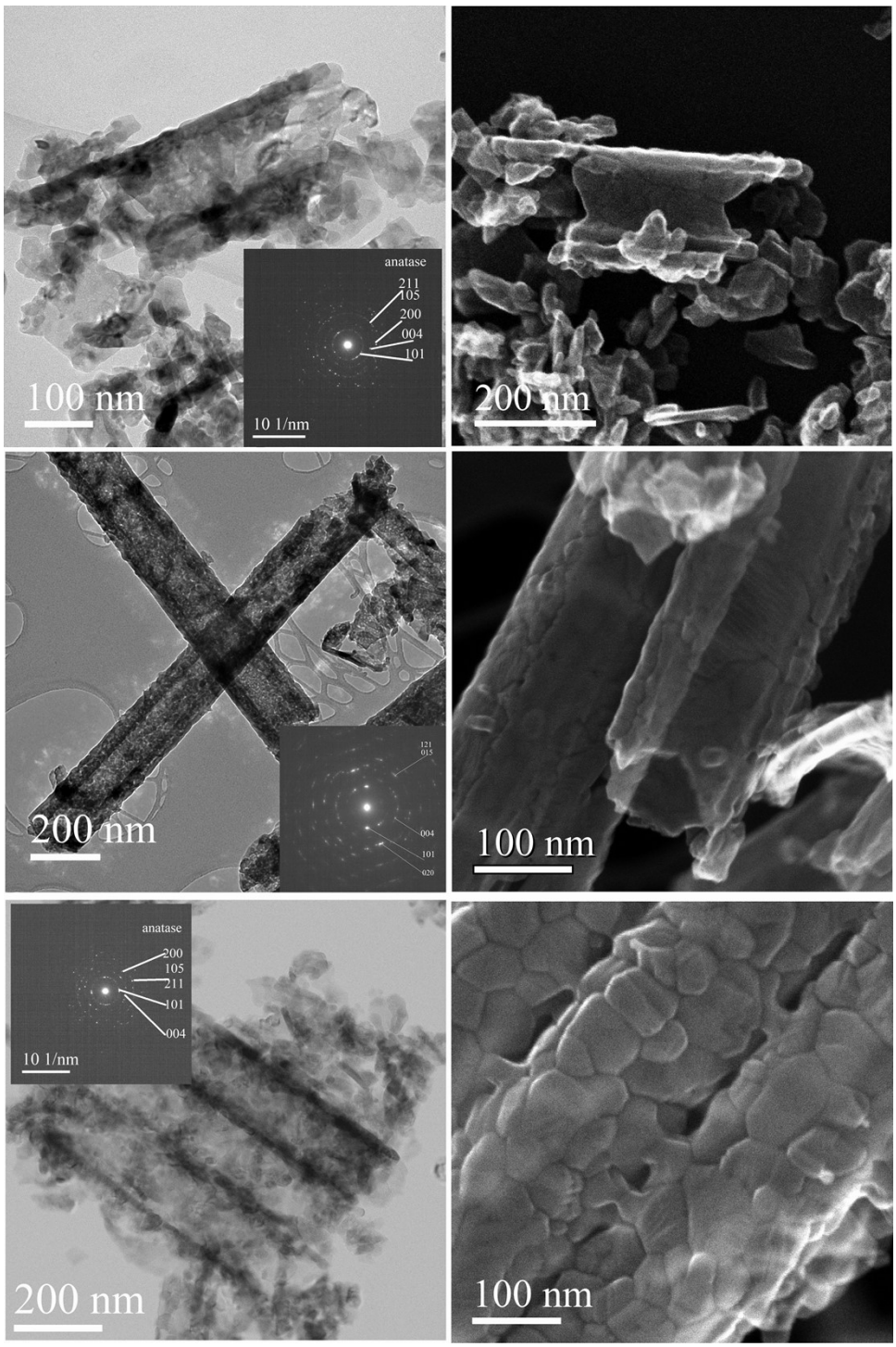

Figure S5: Low-magnification STEM images of nanotube fragments of (a,b) TNT, (c,d) V-TNT, (e,f) Ce-TNT. The inserts correspond to SAED patterns confirming the presence of anatase.

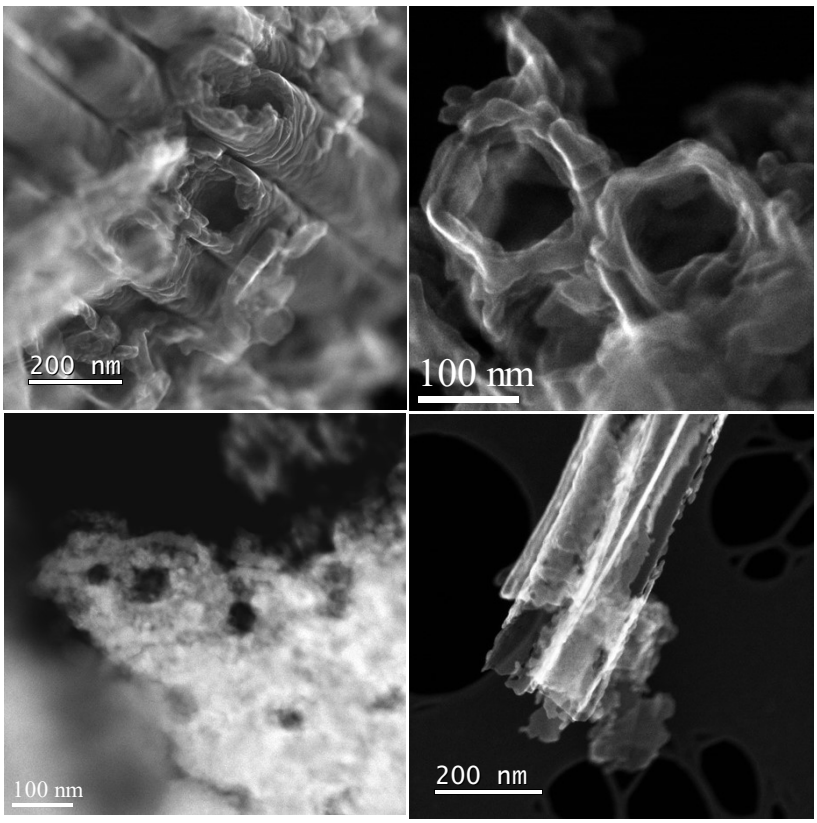

Figure S6: (a) STEM image of nanotube in TNT (nanotube diameter of 180 nm). (b) STEM images of a single-walled region of nanotube in Ce-TNT acquired at the upper portion of the nanotube (diameter of 113 nm). (c) STEM image of a double-walled nanotube in Ce-TNT acquired at the bottom portion of the nanotube (outer and inner diameters of 170 and 75 nm, respectively). (d) STEM image of nanotubes in V-TNT acquired at the upper part and exhibiting partially disintegrated single-walled nanotube.

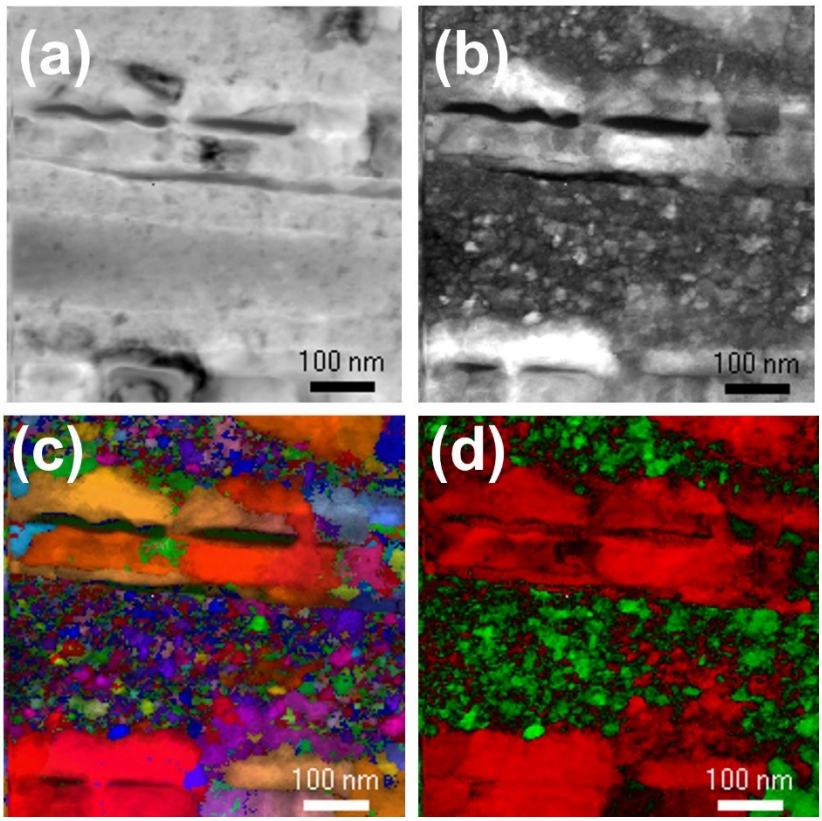

Figure S7. Automated crystal orientation and phase mapping of upper part of TiO_2 nanotubes: (a) Virtual bright field map, (b) index map, (c) overlaying of orientation in z-axis, reliability map and index map, and (d) superposition of phase, reliability and index maps with green and red color labels for rutile and anatase crystallites, respectively.

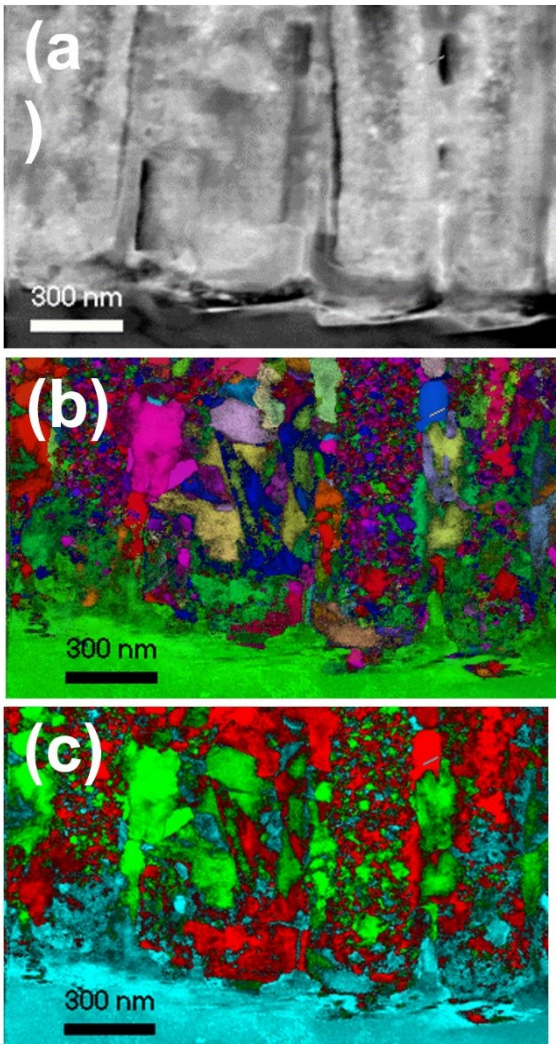

Figure S8. Automated crystal orientation and phase mapping of bottom part of TiO_2 nanotubes: (a) Virtual bright field map, (b) overlaying of orientation in z-axis, reliability map and index map, and (c) superposition of phase, reliability and index maps with blue, green and red color labels for metallic titanium, rutile and anatase crystallites, respectively.

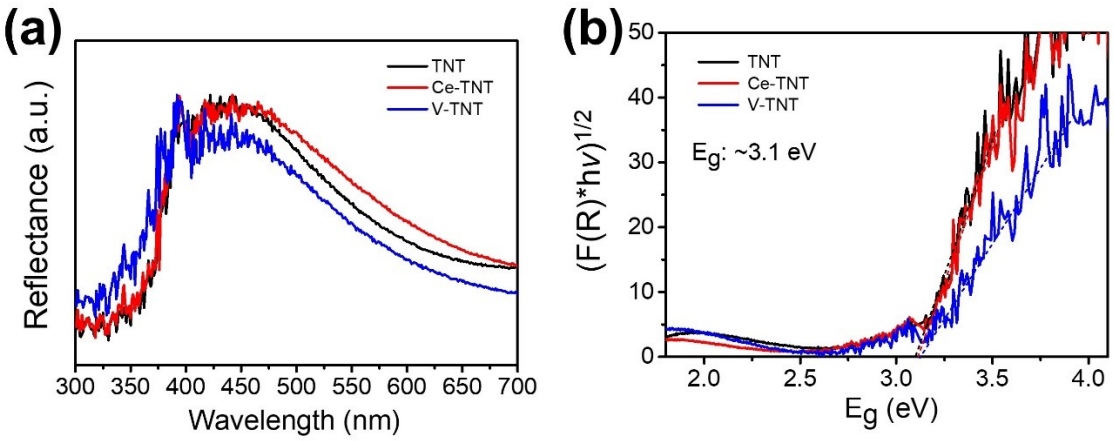

Figure S9: (a) DRS and (b) Tauc plot with the E_g of TNT, TNT/Ce, and TNT/V, respectively.

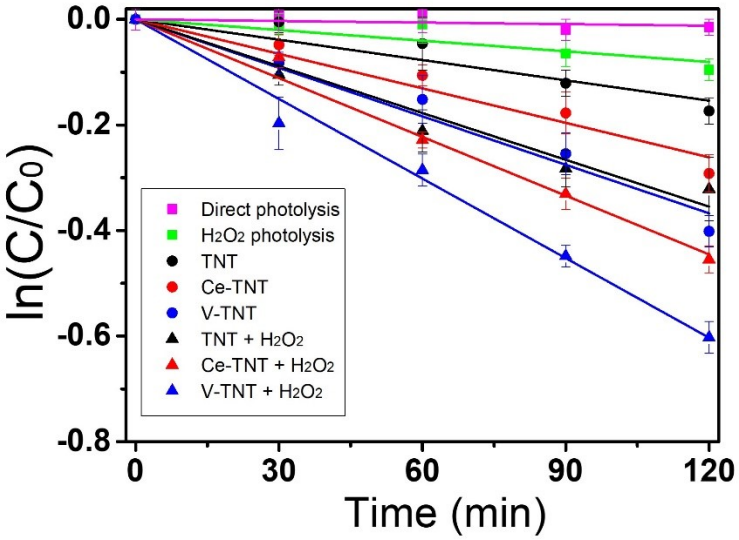

Figure S10: Degradation kinetic curves of CAF (20 ppm) during 2 h UVA irradiation by different photo-induced processes.